A METHOD FOR ANALYZING THE DYNAMIC CHARACTERISTICS OF THE FLANK FACE FRICTION PAIR IN HIGH SPEED MILLING

Minli ZHENG[1*], Minghui ZHANG[1], Bin JIANG[1], and Guisheng YAO[2]
[1] *Harbin University of Science and Technology, National & Local United Engineering Laboratory of High Efficiency Cutting and Tools, Harbin 150080, China*
[2] *Xi' an Aerospace Precision Electromechanical Institute (No.16 Institute), Xi'an 710010, China*
E-mail: fx0zmh@163. com

***ABSTRACT**: During high-speed and intermittent cutting process of milling cutter, the wear of each tooth flank face is different caused by the changing instantaneous radial position angle and cutter vibrations. The cutting motion process of cutter teeth is revealed by solving the cutting trajectory of the cutter tip and the tooth posture under the vibration. The transient angle of normal vectors of the flank face and that of the transition surface is obtained to reflect the dynamic relationship between the friction pairs, and reveal their variation characteristics. The contact position of the dynamic friction pair and relative velocity are investigated to quantitatively describe the time-varying behavior of tooth flank face friction, and a method is proposed to analyze the dynamic characteristics of the flank face friction pair under vibration.*
***KEYWORDS**: high-speed milling cutter, vibration, friction of flank face, difference*

1 INTRODUCTION

The wear of milling cutter flank face affects the cutter service life under the influence of a high-speed, interrupted cutting impact load (Salokyová, 2016). Field investigations show that uneven tooth wear leads to case where the insert is either not fully used or over used. The difference of cutter tooth wear becomes one of the main factors restricting the service life of milling cutter (Jorge et al., 2013; Bushlya et al., 2014; Murali, 2016). But in order to guarantee machining quality, the tooth with the greatest wear is usually regarded as an object for setting the evaluation standard of the milling cutter service life in the actual cutting process, therefore, many inserts are replaced without full utilization, and the cutter utilization rate is generally lower (Iliescu et al., 2006; Toh, 2004). This seriously increases the uncertainty of milling cutter failure, and this uneven wear issue of the milling cutter tooth requires an urgent solution.

At present, research of milling cutter wear is primarily focused on the single tooth wear with different cutting strokes (Zhang et al., 2011). By considering the cutting parameters and other outside factors, Budak restrained the wear of a single cutter tooth by reducing vibrations (Budak, 2006).

Mortazavi et al., (2016) established the prediction model of the tool wear rate and the friction coefficient (Mourad et al., 2017; Mohammed and Ali, 2016; Wang and Huang, 2017). Shen et al. analyzed the friction wear performance on the milling surface by ultrasonic vibration assisted machining (Liu et al., 2008). Existing research explored the form and mechanism of friction wear, and the corresponding laws and characteristics were obtained. But the high speed milling cutters often have multiple teeth cutting, and improving the uneven wear of multiple teeth to ensure high efficiency remains to be studied.

The milling cutter friction under vibration is one of the primary control factors that reduces cutter wear and service performance. The initial stage of wear is the key period for the friction pair between the tooth flank face and the transition surface, which is transferred from the high pair contact to the low pair contact. At this stage, the time-varying behavior of friction wear determines the wear evolution, which has an influence on the service life of the milling cutter. Research of the time-varying behavior of initial friction wear and the difference of flank faces are important steps to reveal the formation and evolution process of uneven wear of cutter teeth.

2 CUTTING MOTION OF CUTTER TOOTH UNDER THE VIBRATION

2.1 Trajectory of cutter tip

The global coordinate system O_g-$X_gY_gZ_g$ is set up, in which the dynamic friction pair of the tooth flank face, time-varying behavior sequences of friction and vibration of the flank face are described. The origin O_g is the intersection point of

the two sides of the workpiece and upper surface of workpiece, the X_q-axis is along the cross feed direction, Y_q-axis is along the feed direction and Z_q-axis is along the axial direction of the machine tool spindle. O_q-$X_qY_qZ_q$ represents the coordinate system according to the right-hand rule (Cosma, 2015). The local coordinate system O_t-$a_tb_tc_t$ fixed on the ideal milling cutter is set up, which the origin O_t is the center of the circle of cutter tips, O_ta_t, O_tb_t and O_tc_t are parallel to O_gX_g, O_gY_g and O_gZ_g, respectively. Under vibration, the offset of the milling cutter needs to be considered, with the ideal cutter local coordinate system origin changing to the point O_t^v. Thus the local coordinate system fixed on the milling cutter under the vibration O_t^v-$a_t^vb_t^vc_t^v$ is established, where c_t^v-axis denotes the tool revolving axis after vibration, a_t^v-axis, b_t^v-axis and c_t^v-axis are the migrated positions of a_t-axis, b_t-axis and c_t-axis, respectively. Meanwhile, the local coordinate system O_i-$a_ib_ic_i$ attached to the ith tooth is set up, in which the cutter tip is regarded as the coordinate origin, a_i-axis is along the cutting velocity direction, b_i-axis is along the direction of level steering angle. O_ib^i intersects with the ith cutting edge and has a level steering angle with O_tb_t. Coordinate systems of milling cutter cutting motion under vibration are shown in Figure 1.

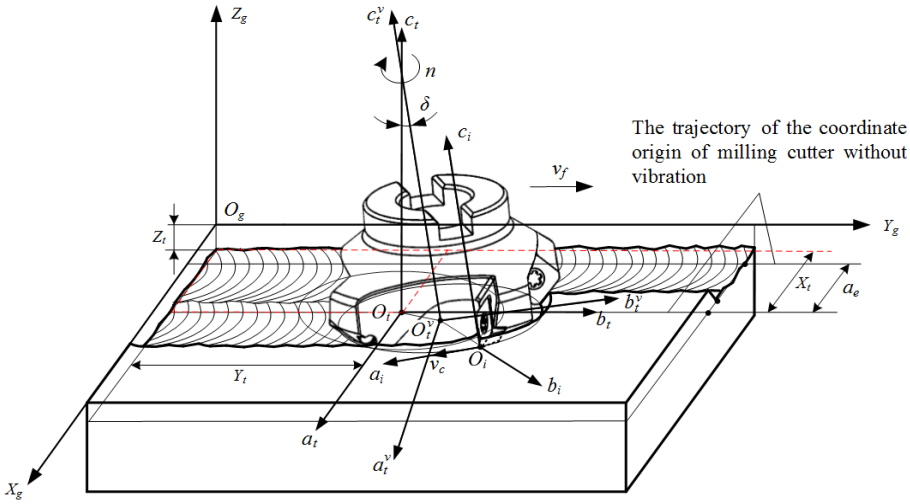

Figure 1. Coordinate systems of cutting motion of milling cutter

As shown in Figure 1, n is the spindle speed, R is the cutter radius, v_f is the feed velocity, a_e is the cutting width, a_p is the cutting depth.

The coordinates of the cutter coordinate origin O_t in the global coordinate system without vibrations can be represented by:

$$X_t = sa_e - R, Y_t = v_f t - R, Z_t = -a_p \qquad (1)$$

where s is the number of tool path intervals.

According to the Fig. 1, the transformation relation between the ideal cutter coordinate system and the cutter coordinate system after vibration is shown in Figure 2.

As shown in Figure 2, δ is the offset angle between O_tc_t and $O_t^vc_t^v$, α is the angle between the O_tc_t and the $O_t^vc_t^v$ projected on the $c_tO_tb_t$ plane, β is the angle between the $O_t^vc_t^v$ and theO_t^v c_t^v projected on the $c_tO_tb_t$ plane. α andβ can be represented as follows:

$$\alpha = \arctan\left(S_Y / (l - S_Z)\right) \qquad (2)$$

$$\beta = \arccos \frac{2l^2 - 2lS_Z^2 + 2S_Y^2}{2\sqrt{(l-S_Z)^2 + S_Y^2 + S_X^2} \cdot \sqrt{l^2 + S_Y^2}} \qquad (3)$$

where SX, SY and SZ are components of the cutter vibration displacement on the directions of Xg-axis, Yg-axis and Zg-axis, respectively.

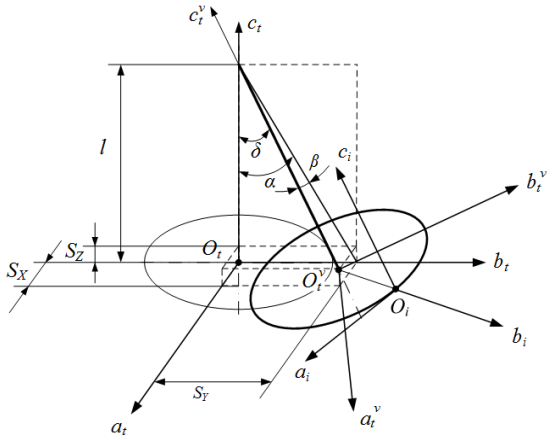

Figure. 2 Transformation relation of cutter tooth cutting motion under vibration

The milling cutter tooth coordinate system, as a co-moving coordinate system, rotates along the axial direction with time t (Zheng et al., 2009), and the homogeneous expression of tool tip trajectory of the ith tooth in the tooth coordinate system transforms is

$$[a_0, b_0, c_0, 1]^T = [R\sin\varphi,\ R\cos\varphi,\ \Delta z_i,\ 1]^T \quad (4)$$

where ω is angular velocity, φ_0 is the initial phase angle, and Δz_i is the axial installation error of ith tooth.

So at t time, the cutter tip trajectory equation of ith tooth can be obtained by rotation matrix M_1.

$$M_1(\omega, \theta_{pi}, t) = \begin{bmatrix} \cos(\omega t - \theta_{pi}) & \sin(\omega t - \theta_{pi}) & 0 & 0 \\ -\sin(\omega t - \theta_{pi}) & \cos(\omega t - \theta_{pi}) & 0 & 0 \\ 0 & 0 & 1 & 0 \\ 0 & 0 & 0 & 1 \end{bmatrix} \quad (5)$$

$$M_2(\alpha, \beta, t) = \begin{bmatrix} \cos\beta(t) & 0 & -\sin\beta(t) & 0 \\ -\sin\alpha(t)\sin\beta(t) & \cos\alpha(t) & -\sin\alpha(t)\cos\beta(t) & 0 \\ \cos\alpha(t)\sin\beta(t) & \sin\alpha(t) & \cos\alpha(t)\cos\beta(t) & 0 \\ 0 & 0 & 0 & 1 \end{bmatrix} \quad (6)$$

$$M_3(S_X, S_Y, S_Z, t) = \begin{bmatrix} 1 & 0 & 0 & S_X(t) \\ 0 & 1 & 0 & S_Y(t) \\ 0 & 0 & 1 & S_Z(t) \\ 0 & 0 & 0 & 1 \end{bmatrix} \quad (7)$$

where θ_{pi} is the angle between the ith cutter tooth and the cutter tooth that cuts into the workpiece at first.

The offset of the milling cutter is considered under vibration. According to Figure 2, the c_t-axis is offset to the c_t^v-axis, the offset angle δ is decomposed into a rotation α degree around the a_t-axis and then rotated β degree around the b_t-axis. The rotation matrix M_2 is shown in equation (6).

The milling cutter generates offset by the vibration, and the transformation matrix M_3 from O_t^v-$a_t^v b_t^v c_t^v$ coordinate system to O_t-$a_t b_t c_t$ coordinate system is shown in equation (7).

As the tool feeds along the Y_g direction, the cutter coordinate system transforms to the global coordinate system at t time can be expressed as

$$M_4(v_f, a_e, a_p, t) = \begin{bmatrix} 1 & 0 & 0 & X_t \\ 0 & 1 & 0 & Y_t \\ 0 & 0 & 1 & Z_t \\ 0 & 0 & 0 & 1 \end{bmatrix} \quad (8)$$

Therefore, based on the cutter's feed motion, rotary motion and cutter vibration, the total transformation matrix of the tooth coordinate system and the global coordinate system can be written in matric form as

$$M = M_4 \times M_3 \times M_2 \times M_1 \quad (9)$$

The trajectory of cutter tip under the vibration can be calculated with equations (4) and (9).

$$[X_{Oi}, Y_{Oi}, Z_{Oi}, 1]^T = M \times [a_0, b_0, c_0, 1]^T \quad (10)$$

2.2 Position and posture of milling cutter cutting edge

The cutting attitude of the ith tooth under vibration is shown in Figure 3.

In the Fig. 3, J_c is the analysis reference point where the distance is $a_p/2$ far from the cutter tip on the cutting edge, λ_s is the inclination angle, and κ_r is the cutting edge angle.

The transient cutting attitude of milling cutter is caused by the cutter offset under vibration, so the inclination angle, the entering angle and rake angle will change

$$\lambda_{is}^v = \pi - \arccos \frac{\left| \overrightarrow{n_{Pr}} \cdot \overrightarrow{O_i J_c} \right|}{\left| \overrightarrow{n_{Pr}} \right| \cdot \left| \overrightarrow{O_i J_c} \right|} \quad (11)$$

$$\kappa_{ir}^v = \pi - \arccos \frac{\left| \overrightarrow{n_{Pf}} \cdot \overrightarrow{O_i J_c} \right|}{\left| \overrightarrow{n_{Pf}} \right| \cdot \left| \overrightarrow{O_i J_c} \right|} \quad (12)$$

where $\boldsymbol{n}_{Pr}$ and $\boldsymbol{n}_{Pf}$ are normal vectors of the datum plane and feed plane across reference points without vibration, respectively.

$$\overrightarrow{n_{Pr}} = [a_{npr}, b_{npr}, c_{npr}, 1]^T = [\cos\theta_s, \sin\theta_s, 0, 1]^T \quad (13)$$

$$\overrightarrow{n_{Pf}} = [a_{npf}, b_{npf}, c_{npf}, 1]^T = [0, 0, 1, 1]^T \quad (14)$$

The coordinates of the analysis reference point J_c in the O_i-$a_i b_i c_i$ coordinate system are analyzed.

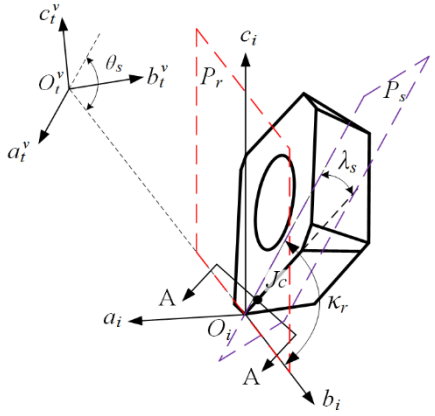

Figure. 3 Cutter tooth posture

$$\begin{cases} a_{iJ_c} = -\dfrac{a_p \sin\lambda_{is}}{2\sin\kappa_{ir}} \\ b_{iJ_c} = \sqrt{\left(\dfrac{a_p\cos\lambda_{is}}{2\sin\kappa_{ir}}\right)^2 - \left(\dfrac{a_p}{2}\right)^2} \\ c_{iJ_c} = a_p/2 \end{cases} \quad (15)$$

The reference point on the cutter tooth coordinate system transforms to the global coordinate system by equation (9). In the global coordinate system, J_c can be obtained by

$$\left[X_{iJ_c}, Y_{iJ_c}, Z_{iJ_c}, 1\right]^T = M \times \left[a_{iJ_c}, b_{iJ_c}, c_{iJ_c}, 1\right]^T \quad (16)$$

Therefore, the directed line segment from the cutter tip to the reference point on the global coordinate system can be expressed as

$$\overrightarrow{O_iJ_c} = [X_{iJ_c} - X_{Oi}, Y_{iJ_c} - Y_{Oi}, Z_{iJ_c} - Z_{Oi}]^T \quad (17)$$

3 MODEL FOR SOLVING FRICTION PAIR OF TOOTH FLANK FACE UNDER VIBRATION

3.1 Equation of milling cutter transition surface

The main cutting edge position of cutter tooth can be determined by the cutting edge angle and the inclination angle. The transition surface is a conical surface formed by the cutting edge sweeping around the rotation center of the milling cutter. The formation of the transition surface in the cutter coordinate system is shown in Figure 4.

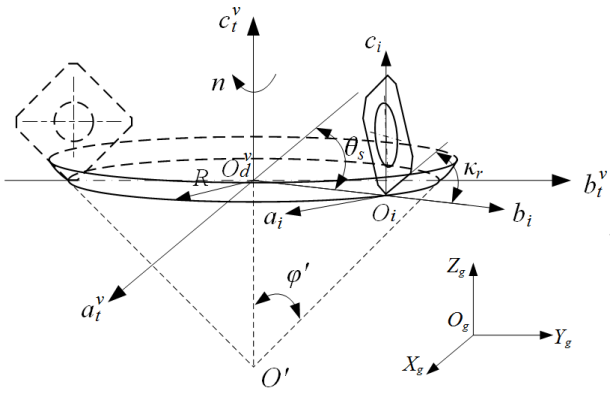

Figure. 4 Formation process of transition surface

As shown in Figure 4, φ' is half the apex angle of the cone. The transition surface equation of the milling cutter in the global coordinate system is obtained in equation (18).

$$\begin{aligned} &(X - sa_e + R(1-\sin\theta_s))^2\cos\kappa_{ir}^v + \\ &(Y - v_f t + R(1+\cos\theta_s))^2\cos\kappa_{ir}^v + \\ &(Z - a_p + \frac{R}{\tan\varphi'})^2(\cos\kappa_{ir}^v - 1) = 0, 0 \le Z \le a_p \end{aligned} \quad (18)$$

Therefore, in the global coordinate system, the normal vector of the transition surface is given as equation (19).

$$\overrightarrow{n_{pt}} = [X_{npt}, Y_{npt}, Z_{npt}, 1]^T \quad (19)$$

3.2 Equation of of flank face

According to Figure 3, the section plan is along the A-A direction; the theoretical contact position of vectors, which is between the transition surface and the flank face is set to the point J, and the friction pair of flank face under the vibration is shown in Figure 5.

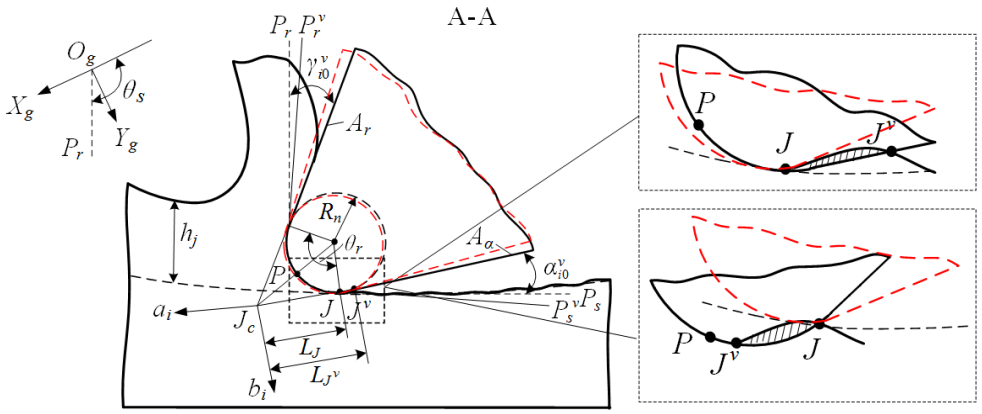

Figure. 5 Friction pair of flank face under vibration

In Figure 5, R_n is the edge radius, θ_r is the central angle of the cutting edge circle, L_J is the theoretical friction contact point position, and P is the end point of cutting edge. Under vibration, the contact point between the flank face and the workpiece is changed from point J to point J^v, and

the position of the friction contact point of the flank face becomes L_{Jv}.

The flank face equation of any point (X_{i0}, Y_{i0}, Z_{i0}) on the tooth flank face is shown in equation (20). In the equation, (X_{iJ}, Y_{iJ}, Z_{iJ}) denotes the coordinates of point J in the global coordinate system, calculated by equation (21) and (22). Thus, the normal vector of the flank face equation of the cutter tooth is obtained, as shown in equation (23).

The cutting posture of the milling cutter under vibration is changing constantly, and the contact profile of cutter tooth friction becomes curved surface of cutting edge circle and flank face. The equation of cutting edge circular surface is shown in equation (24). In equation (24), (X_{iJ}, Y_{iJ}, Z_{iJ}) ${\alpha_{i0}}^{v}$ denotes the instantaneous the relief angle of the ith tooth, calculated by equation (25).

$$\left(Y_{iJ}\frac{a_p}{2}(1-\cos\frac{\theta_r}{2})-Z_{iJ}\frac{a_p}{2}\sin\lambda_{is}^{v}\sin\kappa_r\sin\frac{\theta_r}{2}\right)(X_i-X_{i0})+$$
$$\left(X_{iJ}\frac{a_p}{2}(1-\cos\frac{\theta_r}{2})-Z_J\frac{a_p}{2}\cos\lambda_{is}^{v}\cos\kappa_{ir}^{v}\sin\frac{\theta_r}{2}\right)(Y_i-Y_{i0})+ \quad (20)$$
$$\left(X_{iJ}\sin\lambda_{is}^{v}\sin\kappa_{ir}^{v}\sin\frac{\theta_r}{2}-Y_{iJ}\cos\lambda_{is}^{v}\cos\kappa_s^{v}\sin\frac{\theta_r}{2}\right)(Z_i-Z_{i0})=0$$

$$[X_{iJ},Y_{iJ},Z_{iJ},1]^T=M_i\times M_{i4}\times[a_{iJ},b_{iJ},c_{iJ},1]^T \quad (21)$$

$$(a_{iJ},b_{iJ},c_{iJ})=\left(-\frac{a_p\sin\lambda_{is}}{2\sin\kappa_{ir}}-R_n\tan\frac{\theta_r}{2}\cos\alpha_{i0},\sqrt{\left(\frac{a_p\cos\lambda_{is}}{2\sin\kappa_{ir}}\right)^2-\left(\frac{a_p}{2}\right)^2}-R_n\tan\frac{\theta_r}{2}\cos\gamma_{i0},\frac{a_p}{2}\right) \quad (22)$$

$$\vec{n}_{A\alpha}=(X_{nA\alpha},Y_{nA\alpha},Z_{nA\alpha})=\begin{pmatrix}Y_{iJ}\frac{a_p}{2}(1-\cos\frac{\theta_r}{2})-Z_{iJ}\frac{a_p}{2}\sin\lambda_{is}^{v}\sin\kappa_r\sin\frac{\theta_r}{2},\\ X_{iJ}\frac{a_p}{2}(1-\cos\frac{\theta_r}{2})-Z_J\frac{a_p}{2}\cos\lambda_{is}^{v}\cos\kappa_{ir}^{v}\sin\frac{\theta_r}{2},\\ X_{iJ}\sin\lambda_{is}^{v}\sin\kappa_{ir}^{v}\sin\frac{\theta_r}{2}-Y_{iJ}\cos\lambda_{is}^{v}\cos\kappa_s^{v}\sin\frac{\theta_r}{2}\end{pmatrix} \quad (23)$$

$$\left(X-\left(\frac{R_n}{\sin\theta_r/2}\cos(\frac{\theta_r}{2}+\alpha_{i0}^{v})\right)\right)^2+\left(Y-\left(\frac{R_n}{\sin\theta_r/2}\cos(\frac{\theta_r}{2}+\gamma_{i0}^{v})\right)\right)^2+\left(Z-a_p/2\right)^2-R_n^2=0 \quad (24)$$

$$\alpha_{io}^{v}=\arccos\frac{\left|(M_i\times\vec{n}_{ps})\cdot(M_i\times\vec{n}_{A\alpha})\right|}{\left|M_i\times\vec{n}_{ps}\right|\cdot\left|M_i\times\vec{n}_{A\alpha}\right|} \quad (25)$$

where $\boldsymbol{n}_{Ps}$ is the normal vector of the cutting plane across reference points, and the normal vector in the O_t-$a_tb_tc_t$ coordinate system can be written as follows:

$$\vec{n}_{Ps}=[a_{nps},b_{nps},c_{nps}]=\left[\frac{a_p}{2},0,\frac{a_p\cot\kappa_r^{v}}{2}\right] \quad (26)$$

Thus, the normal vector of equation of cutting edge circular surface in the global coordinate system is

$$\vec{n}_F=M_i\times M_{i4}\times[a_{nF},b_{nF},c_{nF},1]^T \quad (27)$$

$$(a_{nF},b_{nF},c_{nF})=(F_{ai}(a_{i0},b_{i0},c_{i0}),F_{bi}(a_{i0},b_{i0},c_{i0}),F_{ci}(a_{i0},b_{i0},c_{i0})) \quad (28)$$

According to equation (23) and (27), the vector at any point on the flank face or cutting edge circle is given as equation (29).

$$\begin{cases}\vec{n}_A=M\times[a_{nA\alpha},b_{nA\alpha},c_{nA\alpha},1]^T,\ a_i\geq a_{iJ}\\ \vec{n}_A=M\times[a_{nF},b_{nF},c_{nF},1]^T\ ,\ a_i<a_{iJ}\end{cases} \quad (29)$$

3.3 Model of dynamic friction pair of milling cutter tooth flank face

By solving the equation of the cutter flank and the transition surface, the friction pair model between transition surface and cutter flank face is established. The dynamic relationship between the milling cutter transition surface and the flank face is revealed by using the normal vector of two plane, equation (19) and the (29). The characteristic vectors of friction pair is shown in Figure 6.

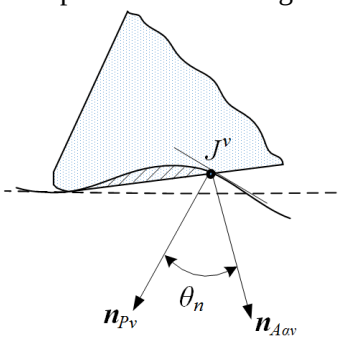

Figure. 6 Characteristic vectors of friction pairs under vibration

As shown in Fig. 6, θ_n is the angle between the two transient vectors $\boldsymbol{n}_{pv}$ and $\boldsymbol{n}_{A\alpha v}$. The transient vector angle θ_n is obtained for the dynamic equations of the flank face and the transition surface and the normal vector of friction pair. θ_n can be described as follows:

$$\theta_n = \arccos \frac{\left| \overrightarrow{n_{p^v}} \cdot \overrightarrow{n_{A_\alpha}} \right|}{\left| \overrightarrow{n_{p^v}} \right| \left| \overrightarrow{n_{A_\alpha}} \right|} \quad (30)$$

In equation (30), the flank face and transition surface of the milling cutter under vibration is in a dynamic change state. Because of the difference of the influence of the vibration on each cutter tooth and the existence of the cutter tooth pitch error, the contact position with the flank face is different. The contact characteristic of the transient vector angle is not the same, which leads to the difference of the friction pairs of cutter teeth.

3.4 Characteristic parameters for friction pair of cutter tooth flank face under vibration

Through the coordinate transformation, the distance from cutter tooth flank face to the reference contact point under the vibration can be expressed as follows:

$$L=\sqrt{(X_{J^v}-X_{Jc})^2+(Y_{J^v}-Y_{J_c})^2+(Z_{J^v}-Z_{J_c})^2} \quad (31)$$

when the friction contact point of flank face is at the cutting edge, $L_{Jv}=-|L_{Jv}|$, when the contact point at the cutter tooth flank face, $L_{Jv}=|L_{Jv}|$.

According to the normal pressure and the transient velocity of each point on the contact surface between the flank face and the workpiece, the friction work is received, and the wear volume in a unit time can be expressed as

$$Q_\alpha = \eta P_\alpha(t) = \eta \sum_{i=1}^{Z} [\mu F_{n\alpha}(t) v^v_{wo\alpha i}(t)] \quad (32)$$

where P_α denotes the consuming power of flank face friction, $F_{n\alpha}$ denotes the transient normal pressure, μ denotes the friction coefficient between the cutter and workpiece surface, and η denotes the coefficient of wear energy efficiency.

Any change of the transient normal pressure in the contact area between the flank face and the workpiece will lead to the change of the contact position of the friction pair, thereby causes the change of friction force. Therefore, the wear volume of the flank face has changes dynamically in any unit time.

In the global coordinate system, v_c^v denotes the cutting speed of milling cutter tooth under vibration. Suppose that the velocity component of v_c^v in feed profile is v_{co}, as shown in Figure 7, v_c^v can be expressed as

$$v_c^v = \sqrt{v_{co}^2 + v_Z^2} \quad (33)$$

$$v_{co} = \sqrt{v_c^2 + v_X^2 + v_Y^2} \quad (34)$$

As shown in Figure 7, v_w is the resultant speed of v_{co} and v_f, v_X and v_Y are vibration speed in the X_g and Y_g directions, respectively, v_{XY} is the resultant speed of v_X and v_Y in the feed plane, v_w^v is the resultant speed of v_{XY} and v_w. θ_0 is the start radial immersion angle in cutting, θ_q is the radial immersion angle, θ_i is the rotation angle of the ith tooth, which start with θ_0, θ_w is the angle of v_c and v_f , θ_m is the angle of v_{co} and X_g direction, and θ_w^v is the angle of v_w^v and v_f.

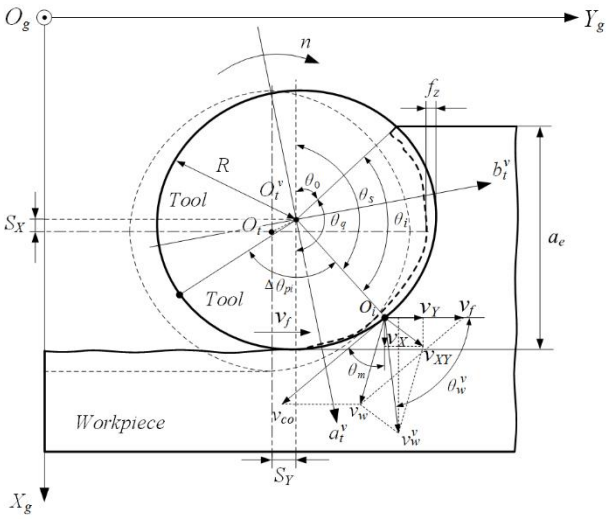

Figure. 7 Cutting motion mode and cutting speed decomposition of milling cutter

The velocity of cutter tooth in X_g direction can be expressed as

$$v_w^v \cdot \sin\theta_w^v = v_{co}\cos\theta_m \quad (35)$$

The velocity of cutter tooth in Y_g direction can be expressed as

$$v_w^v \cdot \cos\theta_w^v = v_f - v_{co}\sin\theta_m \quad (36)$$

And, the velocity of cutter tooth in the feed profile is calculated using equation (35) and equation (36) as follows:

$$v_w^v = \sqrt{{v_f}^2 + {v_{co}}^2 - 2v_f \cdot v_{co}\sin\theta_m} \quad (37)$$

With the change of tooth friction position, the relative speed among the friction pairs is changed. According to the velocity component of the friction contact point on the milling plane under vibration,

the velocity of friction contact point relative to the workpiece is as shown in equation (38).

$$v_{wo}^{v} = \sqrt{v_{w}^{v2} + v_{Z}^{2}} \tag{38}$$

From equation (38), the friction velocity of flank face changes constantly with the changes of the angle θ_w^v. To describe the contact condition of the friction contact point, the velocity of the friction contact point needs to transfer into friction velocity on the cutter flank face. The friction contact point velocity of the flank face can be expressed as,

$$v_{woα}^{v} = v_{wo}^{v} \cdot \cos\alpha_{0}^{v} \tag{39}$$

The friction contact point position and its relative speed are two critical characteristic parameters that directly determine friction time-varying behavior under vibration. These parameters reflect the characteristics of the cutter geometry motion and the process of friction wear. Therefore, using location and relative speed of the flank friction pairs, the formation mechanism of the differences of friction wear could be quantitatively analyzed.

4 EVALUATION METHOD FOR THE DIFFERENCE OF FLANK FACE WEAR FOR EACH CUTTER TOOTH

According to the above analysis, a calculation method of cutter flank face vibrational friction time-varying behavior is proposed based on ISO15641, as shown in Figure 8.

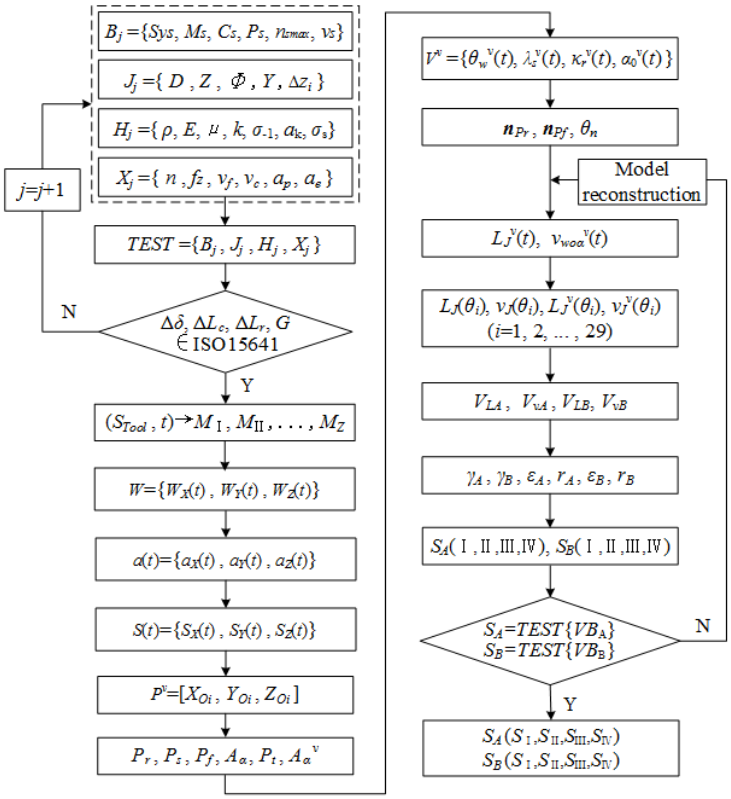

Figure. 8 Calculation method of flank face friction of cutter teeth under vibration

As shown in Figure 8, B is the characteristic uparameter set of the machine tool, which includes: machine operating system Sys, machine weight M_s, machine table dimensions C_s, spindle motor power P_s, the highest spindle speed n_{smax}, and feed speed v_s. J is the cutter structure design set, which includes: teeth distribution Φ and tooth root structure Y. H is the cutter material properties set, which includes: material density ρ, elasticity modulus E, Poisson ratio μ, strength coefficient k, fatigue strength σ_{-1}, material ductility a_k, and yield strength σ_s. X is the cutting conditions set, which includes: rotational speed n, each tooth feed f_z, feed speed v_f, cutting depth a_p and cutting width a_e. S_{Tool} is the behavior of cutter vibration, which includes: cutter vibration signal in cutting of each tooth M_Z (Z=I, II, III, IV). W is the time-domain characteristic of vibration, which includes: time-domain characteristic of X_g-axis, Y_g-axis and Z_g-axis. $a(t)$ is the acceleration equation of milling cutter. $S(t)$ is the transient vibration displacement of milling cutter during cutting process. P^v is the actual

trajectory of tool tip under the vibration. V^{v} is the transient attitude of cutter tooth of milling cutter. $L_J(\theta_i)$ and $L_J^{v}(\theta_i)$ are the sequences of the friction contact point of the flank face under the ideal and vibration conditions, respectively. $v_J(\theta_i)$ and $v_J^{v}(\theta_i)$ are the sequences of the contact point speed of the flank face. V_L and V_v are the dispersion degrees of the friction contact position and contact point speed of flank face, respectively. γ_L and γ_v are the correlation degrees of the friction contact position and contact point speed of flank face, respectively. ε_L and ε_v are the absolute correlation degrees of the friction contact position and contact point speed of flank face, respectively, and r_L and r_v are the relative relation degrees of the friction contact position and contact point speed of flank face.

Based on the cutting vibration behavior characteristics, the friction pair characteristic vectors of the flank face are obtained by recognizing and calculating dynamic cutting behaviors. The calculation model of friction characteristic parameters under vibration indicates the time-varying behavior of flank face friction pair.

5 SUMMARY

The models of the tooth cutting behavior and the dynamic friction pair of the tooth flank face are established under the vibration to reveal dynamic characteristics of the flank face friction pair. The results show that the characteristic vector, normal force and wear volume of the flank face vary with the contact point position and speed, thereby appearing as different processes for the friction wear of each tooth caused by the vibration, and an evaluation method for the difference of flank face wear for each cutter tooth is proposed.

6 ACKNOWLEDGEMENTS

This study was supported by the National Natural Science Foundation of China under the Grant No. 51375124.

7 REFERENCES

►Budak, E. (2006). Analytical models for high performance milling, Part II: Process dynamics and stability, International Journal of Machine Tools and Manufacture, 46(12), 1489-1499.

►Bushlya, V. M., Gutnichenko, O. A., Zhou, J. M., Ståhl, J.E., Gunnarsson, S. (2014). Tool wear and tool life of PCBN, binderless CBN and WBN-CBN tools in continuous finish hard turning of cold work tool steel, Journal of Superhard Materials, 36(1), 49-60.

►Cosma, M. (2015). Influence of tool orientation in five-axes machining process, Academic Journal of Manufacturing Engineering, 13(1), 18-23.

►Iliescu, D., Gehin, D., Nouari, M., Girot, F. (2006). Impact of a diamond coating on tool wear behaviour during dry machining of a multidirectional composite materials, Journal De Physique IV, 134, 1201-1206.

►Jorge, L., García, A., Alejandro, A. I. (2013). Problems in the implementation process of advanced manufacturing technologies, The International Journal of Advanced Manufacturing Technology, 64, 123-131.

►Liu, A. M., Shen, H., Kruth, J. P. (2008). Mechanism of the tool flank wear influenced by the vibration characteristics of the toolholder system in high speed milling, Chinese Journal of Mechanical Engineering, 44(4), 63-68.

►Mohammed, B., Ali, B. (2016). Modeling the problem of contact and friction between a body elastic and rigid foundation, Mathematical Modelling of Engineering Problems, 3(4), 191-194.

►Mortazavi, V., Khonsari, M. M. (2016). On the prediction of transient wear, Journal of Tribology, 138(4), 041604.

►Mourad, D., El Hedj, O., Rachid, L., Ahmed, M. (2017). Experimental characterization of the Heat Affected Zone (HAZ) properties of 100Cr6 steel joined by rotary friction welding method, Mathematical Modelling of Engineering Problems, 4(1), 43-47.

►Murali, D. (2016). Comparison of adaptive neuro-fuzzy based PSS and SSSC controllers for enhancing power system oscillation damping, Advances in Modelling and Analysis C, 71(1), 24-38.

►Salokyová, Š. (2016). The occurrence of mechanical vibration due to changing thickness of splinter during milling, Academic Journal of Manufacturing Engineering, 14(2), 46-51.

►Toh, C. K. (2004). Vibration analysis in high speed rough and finish milling hardened steel, Journal of Sound & Vibration, 278(1), 101-115.

►Wang, Y., Huang, D. K. (2017). Effect of heat treatment temperature on the structure and tribological properties of nanometer lanthanum borate, International Journal of Heat and Technology, 35(1), 53-58.

►Zhang, H., Chen, W. Y. (2011). Milling tool rapid selection based on statistical law of initial wear, Journal of Mechanical Engineering, 47(11), 191-198.

►Zheng, M. L., Jiang, B., Zhang, W., Liu J. (2009). High speed milling stability of cutter with indexable inserts, Key Engineering Materials, 392-394, 560-564.